Report of the National Reserch Institute for Earth Science and Disaster Prevention, No.47 ; March 1991

550.34:550.398.3

Update on the examination of the seismic observational network of the National Research Institute for Earth Science and Disaster Prevention(NIED) — detection capability and magnitude correction —

by

Maria Teresa MORANDI

Laboratory of Geophysics, University of Los Andes, Venezuela

and

Shozo MATSUMURA*

National Research Institute for Earth Science and Disaster Prevention, Japan

Abstract

The operation of a seismological network must be systematically reviewed, not only in order to maintain it but also to improve its detection and location capability. A method for evaluating detection and location capability was developed by Matsumura in 1984 . Later, Papanastassiou and Matsumura applied the method to the NIED network in 1987, and estimated the capability by using data periods from 1984 to 1985. After that time,the NIED Network was extended, and the number of its stations have increased from 67 to 84 at the present.

In this report, detection and location capability in the present stage of the NIED network is re-estimated. Compared with the previous results, a remarkable improvement of location capability is found in the northern area of the Kanto district. However, a location capability map for earthquakes of magnitude 1.5 shows that the southeastern area, covering the Boso Peninsula is still behind the general progress of the network.

Station corrections for magnitude determination are also examined. The result shows a definite difference in the correction due to ground motion response between the western and the eastern areas.

Key words : icroearthquake observation, Magnitude correction

1. Introduction to the NIED'S Observational Network

The Kanto-Tokai area, with an approximate radius of 200km, is seismically monitored by a high quality digital network of the NIED. Figure 1 shows the geographical distribution of the observation stations of the network covering the Kanto-Tokai area. Observed data are digitized and telemetered to the NIED in Tsukuba Science City through telephone lines. The outputs are transmitted into the digital data processing system and processed by the NIED's exclusive computer system (Matsumura et. al., 1986).

Construction of this NIED Network began in 1978. It includes 4types of

* Earthquake Precursors Research Laboratory, Solid Earth Science Division.

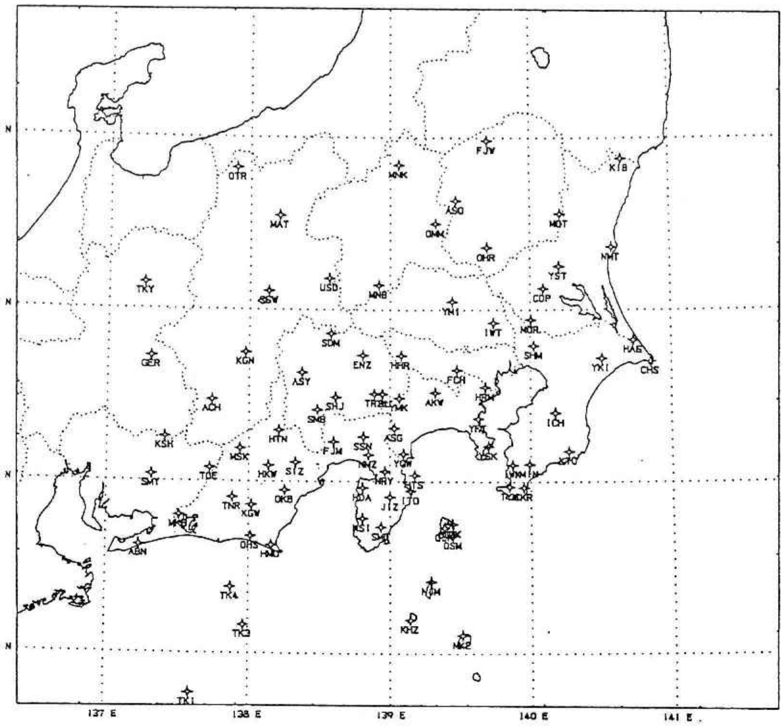

Fig.1 Station distribution of the Kanto−Tokai observational network of the NIED as for September, 1988.

stations for seismic and tilt observations. These types are: surface stations, tunnel stations, shallow borehole stations and deep borehole stations. The standard type of station is a shallow borehole observatory with a depth of 100 meters and a diameter of 4 inches (about 10cm) at the bottom. This type of observation station is equipped with three components of seismographs, and/or two components of tiltmeters. In order to overcome the artificial noise at the surface in and around Tokyo, three deep borehole observatories with depths of from 2300 to 3500 m were constructed. These deep borehole stations reaching the basement rock, are named FCH, IWT and SHM, and their sensor vessels contain seismometers, accelerometers and tiltmeters. The standard seismograph installed is a three component set of a velocity proportional type, with a natural frequency of 1 Hz, a damping constant of 0.7 and a sensitivity of 2.0 V/kine (1 kine $= 10^{-2}$ m/s). A complete outline of the system is presented by Hamada et al. (1985).

Figure 2 shows the variation of monthly earthquake numbers located for the entire period of observation from July, 1979 till June, 1990. From this figure, it is recognized that while unusually active periods sometimes appear, the basic activity is rather constant, and its mean level is noted to be elevated on several occasions, for

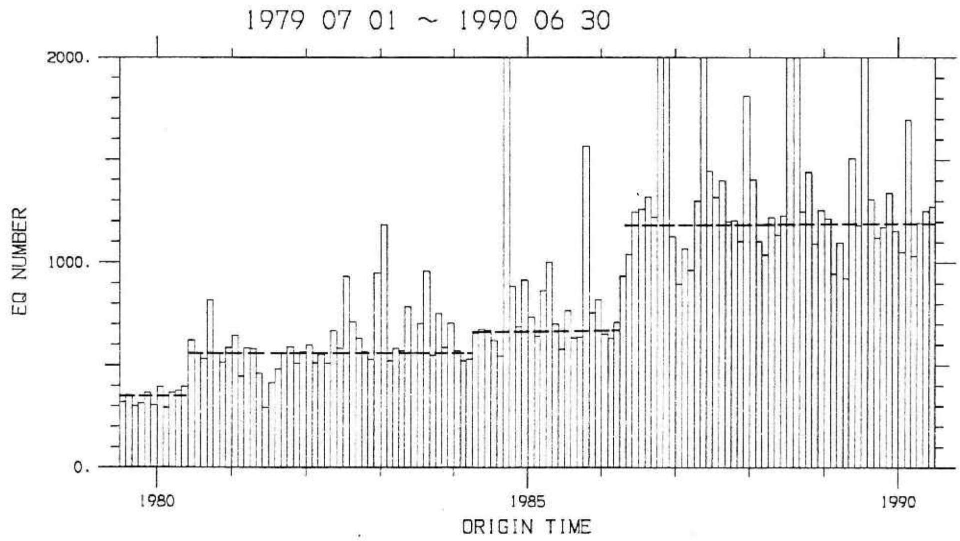

Fig.2 Monthly number of located earthquakes obtained by the NIED observational system.

example, June, 1980; April, 1984; and April, 1986. Such an increase of located earthquake numbers can be attributed to the growth of the network and improvement of the data processing system. The most recent elevation was noted probably because of the installation of the new data processing system, APE(the Analyzing System for Precursors of Earthquakes). This is the reason why we intend to re−estimate the capability of the observation network in the most recent situation.

2. Detectability and Locatability

The term detection−location probability is defined as the ability of a seismic network to detect and locate any earthquake with a magnitude larger than a threshold magnitude and a focal coordinate (X,Y,Z).

Many methods have been developed to estimate detection or location capability of a seismic network. Ringdal (1975) has divided these methods into three categories:

1. The indirect estimation method, which is based on seismic noise studies.
2. The recurrence curve estimation method, which is based on comparison between the true seismicity and the observed detection performance.
3. The direct estimation method, which is based on comparison to a reference observation system.

The method taken up in this work cannot be classified into any of the above categories based on the actual data obtained at each seismic station (Matsumura, 1984; Papanastassiou and Matsumura, 1987). The data period used for the present work is from September, 1988 to June, 1989 and from August, 1989 to March, 1990, with the exception of those periods which include unusual activities and of course periods of inferior operation at each station.

.2 1 Detection Probability at Stations

The essential point of this method is to combine the individual detection capability of single stations. At first, we have to know the detection capabilities of the stations, individually. For each station, it is investigated whether an earthquake could have been detected or not, by plotting its magnitude versus the hypocentral dist ance. As seen in Fig. 3, the areas of detected (circle) and non−detected (cross) earthquakes are clearly distinguished. However, a mixing of both symbols appears around the bordering line. This indicates the possibility of fluctuations of the magnitude estimated at that station, which may be mainly attributed to the difference of the focal mechanism. A broken line separating the circles and crosses is drawn, according to the equation derived by Watanabe (1971), so that it passes and intersects equally both areas. The Watanabe's equation relating the magnitude M to the hypocentral distance R (km), and the maximum amplitude A (kine) is given as:

$$0.85\,(M-2.04\log R) = \log A + 2.50 \quad (R \leq 200\mathrm{km}),$$

$$0.85\,(M-2.04\log R - 0.0018\,(R-200)) = \log A + 2.50 \quad (R > 200\mathrm{km}). \qquad (1)$$

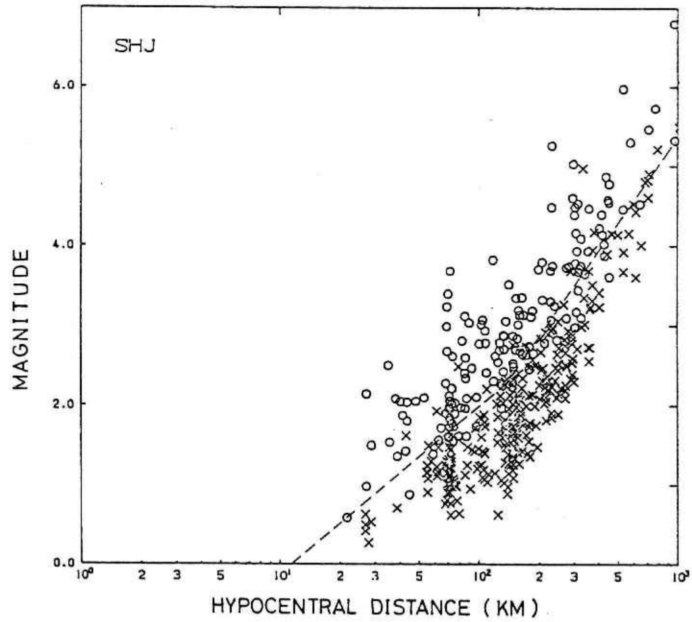

Fig. 3 Plotting of earthquakes on the magnitude versus hypocentral distance coordinate. Circles indicate earthquakes detected at the station 'SHJ', and crosses indicate those non−detected. The broken line is drawn to separate circles from crosses, according to the formula given in Eq. 1 with fixing the value of amplitude A.

By using these equations, Fig. 3 is translated into a new plot with reduced magnitude M' in order to estimate the detection probability of each station:

$$M' = M - 2.04 \log R \qquad (R \leq 200\text{km}),$$
$$M' = M - 2.04 \log R - 0.0018\,(R - 200) \qquad (R > 200\text{km}). \tag{2}$$

Then, the ratios of the number of detected earthquakes to the total number of earthquakes are plotted on the axis of M' for each station. Figure 4 shows the result of such plotting for the same data as those of Fig.3. Here, an approximate line fitting is carried out by introducing a cumulated normal distribution function (Φ) of an analytical form as,

$$p_i\,(M, R) = \Phi\left(\frac{M' - \mu_i}{\sigma_i} \right). \tag{3}$$

The value of M' at $p_i = 50\%$(i.e. $M' = \mu_i$) is directly related to the sensitivity of the station. The smaller the value of μ_i is, the more sensitive the station is. On the other hand, the standard deviation factor σ_i represents the scattering of the symbols across the separating line in Fig.3, as estimated from the slope of the fitted line in Fig.4. The geographical coordinate, altitude, and the values of μ_i and σ_i obtained for each station are summarized in Table 1. The distribution pattern for the values of μ_i is shown in Fig.5, from which we can recognize a distinct tendency, that is, stations in the mountainous area indicate a comparatively high sensitivity, while in contrast, stations around the ocean or plain area indicates a low sensitivity.

2.2 Locatable Probability

The next step is to calculate the locatable probability of the network. The probability P_i that an earthquake could be detected at only i stations can be written as follows:

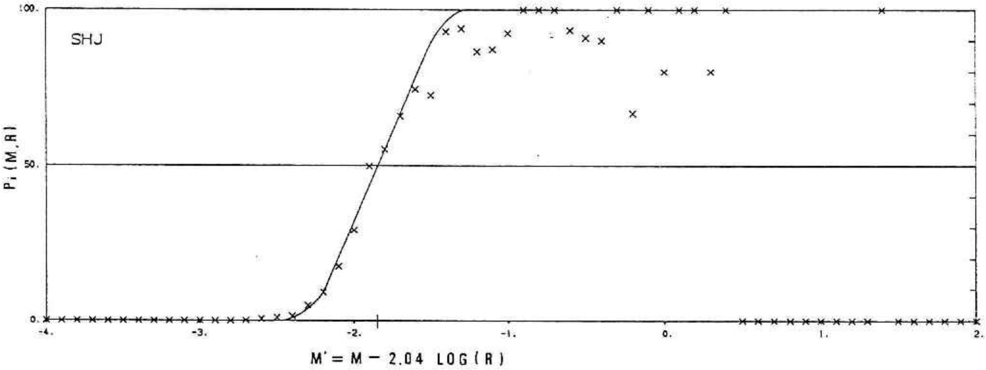

Fig. 4 Detection probability of earthquakes at 'SHJ' as a function of the reduced magnitude M . The continuous line based on the cumulative normal distribution function is fitted to the plotted data.

Table 1 Geographical coordinate, altitude, and the values of μ i and σ i for each station.

STATION	LAT(N)	LON(E)	ALT(Km)	μ	σ
ABN	34.629	137.234	0.040	-1.57	0.49
ACH	35.475	137.738	0.762	-2.06	0.42
AKW	35.520	139.318	-0.010	-1.53	0.31
ASG	35.314	139.028	0.386	-1.67	0.38
ASO	36.631	139.465	0.755	-2.54	0.26
ASY	35.635	138.373	0.800	-1.82	0.51
CDP	36.122	140.093	-0.620	-2.20	0.41
CHS	35.702	140.855	-0.042	-1.00	0.28
CKR	34.967	139.969	-0.661	-1.20	0.37
ENZ	35.736	138.805	0.807	-2.01	0.55
FCH	35.651	139.474	-2.707	-1.79	0.34
FJM	35.233	138.597	-0.059	-1.12	0.24
FJW	35.233	138.597	0.665	-2.04	0.68
GER	35.727	137.305	0.620	-2.08	0.58
GJK	34.734	139.384	0.558	-1.10	0.57
HAS	35.826	140.736	-0.784	-1.32	0.30
HCJ	33.073	139.843	0.036	-0.98	0.46
HDA	34.965	138.805	-0.046	-1.66	0.56
HHR	35.735	138.805	0.595	-2.18	0.38
HKW	35.093	138.138	0.343	-1.74	0.57
HMO	34.630	138.159	-0.061	-0.92	0.38
HRM	35.551	139.679	-0.535	-0.79	0.36
HTN	35.300	138.211	0.855	-1.87	0.76
HTS	35.039	139.172	-0.084	-1.25	0.27
ICH	35.401	140.177	-0.146	-0.91	0.31
ITO	34.949	139.141	-0.087	-1.31	0.29
IWK	35.098	139.871	-0.010	-1.26	0.34
IWT	35.926	139.738	-3.501	-2.08	0.51
JIZ	34.913	138.997	0.263	-1.86	0.50
KGN	35.752	137.972	0.629	-2.00	0.45
KGW	34.863	138.022	0.069	-1.65	0.49
KHZ	34.196	139.139	0.053	-0.72	0.53
KIB	36.878	140.658	0.298	-2.01	0.43
KSH	35.258	137.409	0.343	-2.00	0.55
KTU	35.177	140.269	-0.012	-0.96	0.34
MAT	36.543	138.207	0.406	-1.86	0.36
MIN	35.102	139.990	0.112	-1.26	0.29
MKB	34.801	137.514	-0.038	-1.64	0.51
MKE	34.106	139.510	0.164	-1.20	0.41
MNB	36.141	138.917	0.895	-2.14	0.48
MOR	35.942	140.005	0.001	-0.40	0.43

Table 1 (continued)

STATION	LAT(N)	LON(E)	ALT(Km)	μ	σ
MOT	36.553	140.217	0.140	-2.44	0.23
MSK	35.193	137.939	0.754	-2.06	0.51
NJM	34.420	139.288	0.050	-0.56	0.41
NMT	36.362	140.584	-0.075	-1.11	0.30
NMZ	35.158	138.846	0.114	-1.20	0.32
NRY	35.060	138.963	-0.091	-1.69	0.50
NSI	34.787	138.804	-0.422	-1.74	0.50
ODK	34.755	139.439	0.090	-1.18	0.46
OHR	36.360	139.692	0.244	-2.42	0.22
OHS	34.682	138.015	-0.067	-1.14	0.34
OKB	34.950	138.253	-0.032	-1.44	0.38
OMM	36.497	139.321	0.463	-2.50	0.34
OOH	34.751	139.406	0.412	-1.22	0.41
OSM	34.688	139.443	-0.044	-0.92	0.41
OTR	36.818	137.903	0.575	-1.72	0.41
SDM	35.864	138.577	1.270	-1.80	0.46
SHJ	35.492	138.612	0.880	-1.74	0.43
SHM	35.793	140.023	-2.277	-2.14	0.34
SIZ	35.112	138.330	0.076	-1.79	0.51
SMB	35.416	138.483	0.202	-1.84	0.49
SMD	34.738	138.934	0.013	-1.64	0.61
SMY	35.036	137.316	0.303	-2.02	0.53
SSN	35.262	138.810	0.900	-1.44	0.49
SSW	36.106	138.133	0.987	-1.78	0.37
TKY	36.152	137.255	0.561	-1.53	0.32
TK1	33.765	137.599	-2.202	-0.54	0.51
TK2	33.947	137.757	-1.542	-0.66	0.53
TK3	34.165	137.965	-0.817	-0.14	0.52
TK4	34.385	137.875	-0.722	-0.58	0.38
TNR	34.908	137.885	0.066	-1.66	0.56
TOE	35.078	137.724	0.255	-2.04	0.65
TRU	35.510	138.944	0.565	-1.82	0.52
TR2	35.512	138.887	0.151	-1.78	0.48
TYM	34.971	139.848	0.030	-1.20	0.28
USD	36.181	138.564	0.969	-2.21	0.40
YFT	35.367	139.629	-0.026	-1.10	0.42
YGW	35.163	139.093	0.141	-1.83	0.38
YKI	35.718	140.509	-0.142	-0.96	0.27
YMI	36.048	139.440	-0.052	-1.57	0.29
YMK	35.487	139.063	0.564	-1.92	0.45
YSK	35.208	139.700	-0.189	-1.08	0.29
YST	36.253	140.206	-0.071	-1.98	0.34

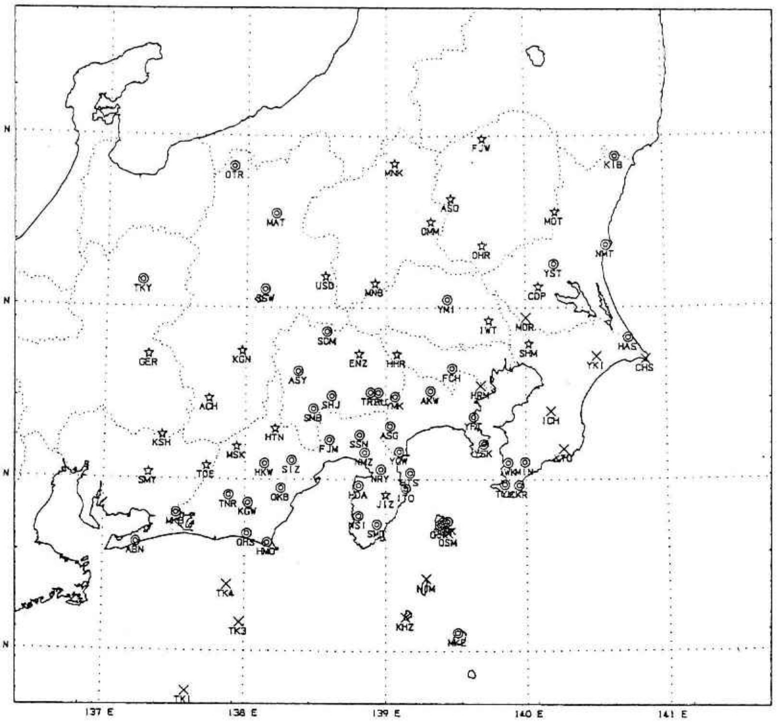

Fig.5 Values of μi for each observatory.
cros : $-1.0 < \mu i$,
double circle : $-2.0 < \mu i \leq -1.0$,
star : $\mu i \leq -2.0$.

$$P_0 = (1-p_1)(1-p_2)\cdots(1-p_N)$$

$$P_1 = p_1(1-p_2)(1-p_3)\cdots(1-p_N) + \cdots p_N(1-p_1)(1-p_2)\cdots(1-p_{N-1})$$

$$P_2 = p_1 p_2(1-p_3)\cdots(1-p_N) + \cdots + p_{N-1} p_N (1-p_1)\cdots(1-p_{N-2})$$

$$\cdots$$

$$P_N = p_1 p_2 p_3 \cdots p_{N-1} p_N, \tag{4}$$

where pj is the probability in Eq.3 that the earthquake could be detected at the j−th station, and N is the total number of stations. In order to determine hypocenters, it is necessary that the earthquake must be detected at more than two stations. Then, the probability satisfying this condition can be given as,

$$P = 1.0 - (P_0 + P_1 + P_2). \tag{5}$$

To calculate the locatable probability of the network, the observation area is divided by a three−dimensional lattice with 10km x 10 km x 10 km elements. It is assumed that an earthquake with a given magnitude occurs at every lattice point. After computing the probability P for each point, we can make a contour map of locatability by taking the area where P indicates a value of 95%.

2.3 Results and Discussion on Detectability and Locatability

By connecting the points where the locatable probability is equal to 95%, we obtained the contours for different depths as shown in Fig.6, and 7(a)~(c). Figure 6 shows the results of the locatability for microearthquakes with various magnitude thresholds estimated on the surface of the Kanto−Tokai observational network. As can be seen, the contour for a threshold magnitude of 1.5 surrounds a big area including the Tokyo Metropolitan area and the Izu Peninsula, but still misses the Boso Peninsula region.

Figure 7 shows a three−dimensional feature of the region under consideration. While for magnitude 1.0, the locatable area is separated into three regions, those areas for magnitudes greater than 1.5 are recognized to compose a continuum. Figures 8(a)~(c) are the similar figures drawn after the results of Papanastassoiou and Matsumura (1987). By comparison of both figures, improvement of locatability becomes clear, especially for the northeastern area of the network.

3. Magnitude Correction

Since Richter proposed the definition of earthquake magnitude based solely on amplitudes of ground motion recorded by seismographs, Richter's magnitude scale

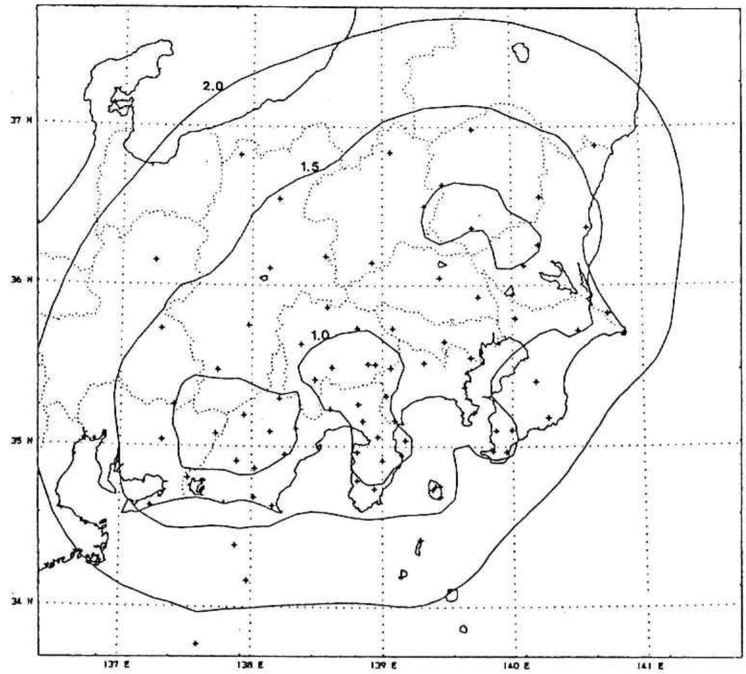

Fig.6 Limits of possibly detecting and locating earthquakes greater than the threshold magnitude. Each boundary line corresponds to the most−outer contour of Fig. 7.

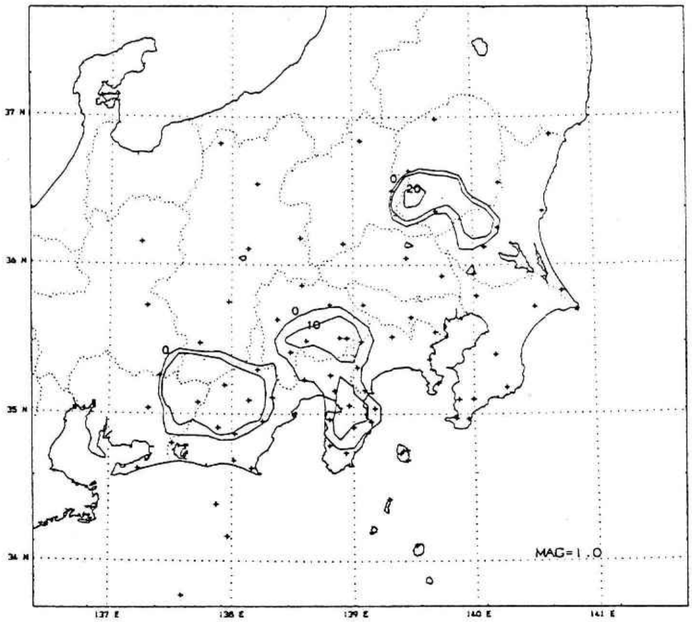

(a) MAG=1.0.

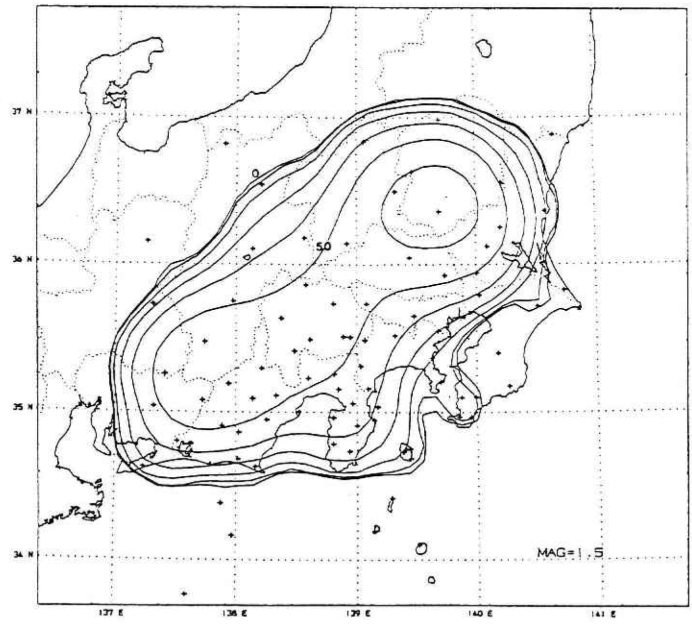

(b) MAG=1.5.

Fig.7 The contours show the three-dimensional feature of the region, inside which earthquakes greater than the threshold magnitude (MAG) are locatable with a probability larger than 95%. The numerals indicate depth of the contours in unit of km.

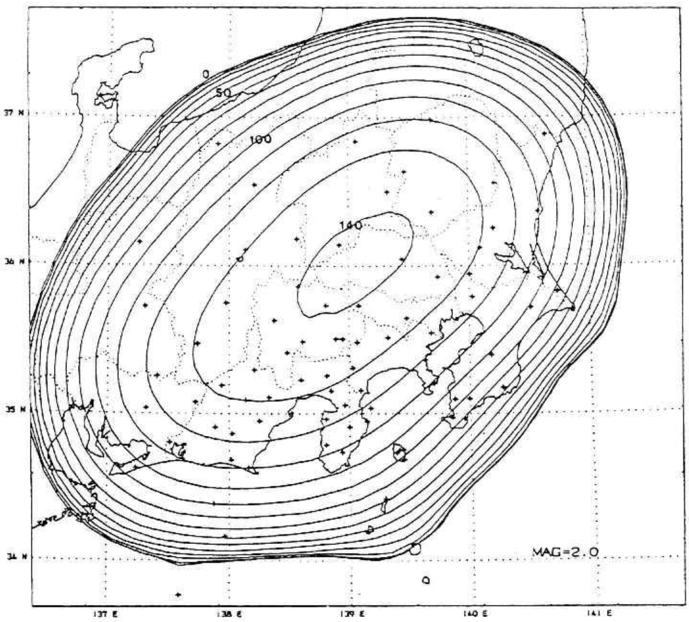

Fig. 7 (continued) (C) MAG=2.0.

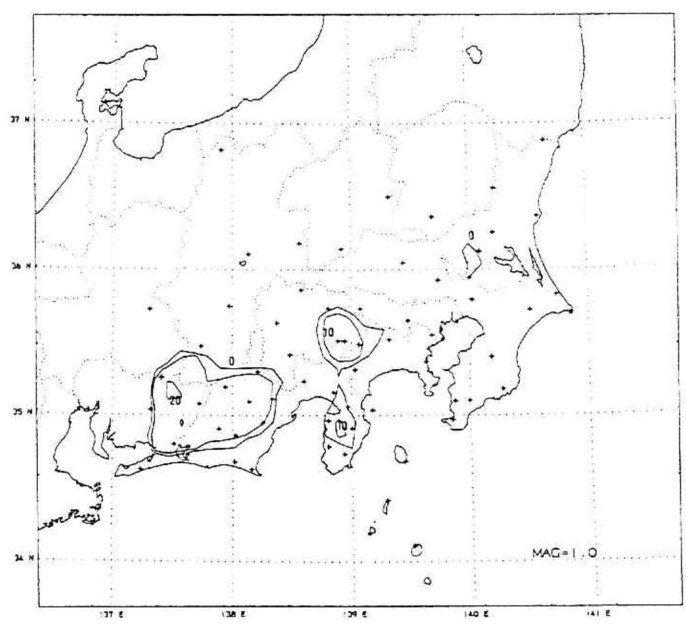

(a) MAG=1.0.

Fig.8 The results given by Papanastassiou and Matsumura (1987) for comparison with Fig.7.

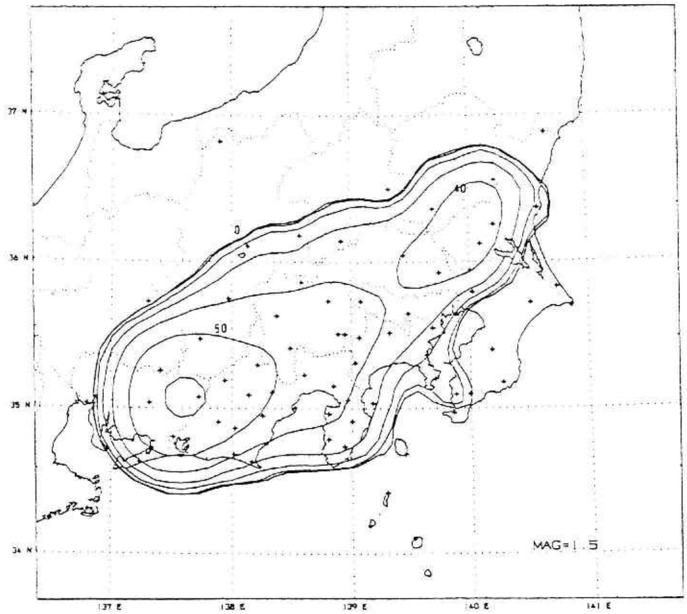

(b) MAG=1.5.

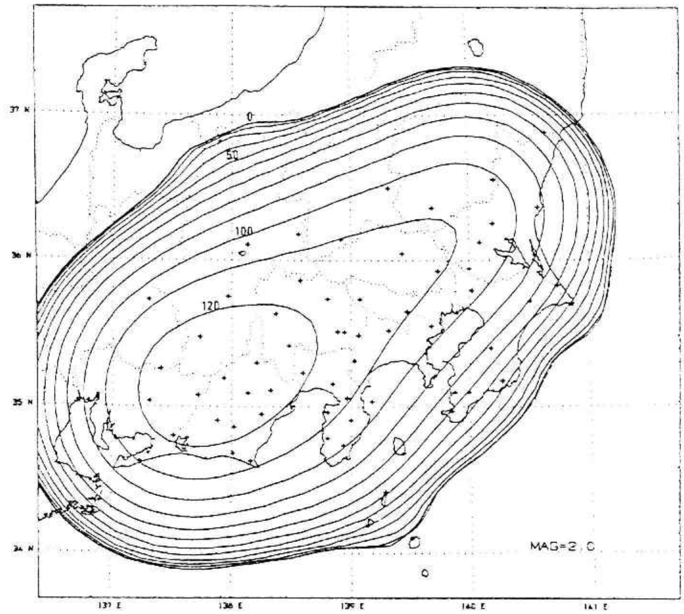

(C) MAG=2.0.

Fig. 8 (continued)

has been widely accepted and the quantification of earthquakes has become an active research topic in seismology. Originally, Richter's magnitude scale was defined for local earthquakes in Southern California, using signals recorded on Wood–Anderson seismographs. Since then, many attempts have been carried out to extend its availability for more distant earthquakes, the utilization of different instrument's records, and so on (Lee and Stewart, 1981) .

In the present case, the magnitude of an earthquake is determined by computing the average of all the estimates obtained at each station. However, the magnitude obtained at each station does not always represent the true magnitude. The wave amplitude observed at a local station may be affected by various factors. Two important factors must be taken into consideration. One is the focal mechanism of the source, and the other is the local site effect. The former may be compensated by taking an average, but the latter is still problematic. Wave amplitude may be strongly affected by the physical property of the rock. For example, high frequency terms of waves are more rapidly attenuated through soft sediment rocks. All these effects will lead to complex results.

So, if it is desirable to make magnitude determination more accurate, it is necessary to introduce a correction factor at each station in order to remove the local effect.

3.1 Method

This work proposes a numerical method to estimate deviations of the magnitude obtained at each local station. The basic idea is very similar to that developed by Maeda (1984) , yet slightly different.

The magnitude M_{ij} observed at the j–th station for the i–th earthquake can be written as,

$$M_{ij} = M_i + c_j + \varepsilon_{ij} , \tag{6}$$

where M_i is the true magnitude of the i–th earthquake ($i = 1 \sim N_e$, N_e is the total number of earthquakes), c_j is a characteristic term of the j–th station ($j = 1 \sim N$, N is the total number of stations), so, $-c_j$ corresponds to the station correction for the magnitude, and ε_{ij} means fluctuation of the magnitude, which may be caused by a difference of the rediation pattern. On the other hand, the magnitude m_i assigned for the i–th earthquake is given as an average of M_{ij} as,

$$\begin{aligned} m_i &= (\sum_j a_{ij} M_{ij}) / (\sum_j a_{ij}) \\ &= M_i + (\sum_j a_{ij} c_j) / n_i + (\sum_j a_{ij} \varepsilon_{ij}) / n_i , \end{aligned} \tag{7}$$

where a_{ij} is an index indicating whether the seismic wave of the i–th earthquake can be detected at the j–th station ($a_{ij}=1$) , or not ($a_{ij}=0$) , and n_i ($= \sum_j a_{ij}$) is the number of stations where the wave was detected. Here, the third term of Eq.7 can be assumed to be approximately zero. Then the magnitude difference ΔM_{ij} between that observed and averaged at the j–th station is given by using Eq.6 and Eq.7 as,

$$\Delta M_{ij} = M_{ij} - m_i$$
$$= c_j + \varepsilon_{ij} - (\sum_k a_{ik} c_k) / n_i, \ (k = 1 \sim N). \tag{8}$$

so,

$$\varepsilon_{ij} = \Delta M_{ij} - c_j + (\sum_k a_{ik} c_k) / n_i. \tag{9}$$

Now, we assume a normal distribution for ε_{ij} as,

$$\exp(-\varepsilon_{ij}{}^2 / 2\sigma_j{}^2), \tag{10}$$

where σ_j is the standard deviation of the magnitude determined at the j−th station, which should be the same parameter introduced in the former chapter. According to the maximum likelihood method for the distridution based on Eq.10, the following function should be minimized by taking the most appropriate values for the parameters

$$f = \sum_i \sum_j \frac{a_{ij}}{\sigma_j{}^2} \left(\Delta M_{ij} - c_j + \frac{1}{n_i} \sum_k a_{ik} c_k \right)^2. \tag{11}$$

By partially differentiating Eq.11 by c_m ($m = 1 \sim N$), and letting it be zero, we obtain,

$$\begin{aligned} &\sum_i a_{im} (c_m - \Delta M_{im}) \\ &+ \sum_i \sum_j \frac{a_{ij} a_{im}}{n_i} \left(\frac{\sigma_m^2}{\sigma_j{}^2} \Delta M_{ij} - \frac{\sigma_m^2}{\sigma_j{}^2} c_j - c_j \right) \\ &+ \sum_i \sum_j \sum_k \frac{a_{ij} a_{ik} a_{im}}{n_i^2} \frac{\sigma_m^2}{\sigma_k{}^2} c_j = 0. \end{aligned} \tag{12}$$

By rearranging these equations, we get a set of linear equations for c_j as,

$$\sum_j h_{mj} c_j = g_m. \tag{13}$$

where

$$h_{mj} = \sum_i \frac{a_{ij} a_{im}}{n_i} \left(1 + \frac{\sigma_m^2}{\sigma_j{}^2} - \frac{\sigma_m^2}{n_i} \sum_k \frac{a_{ik}}{\sigma_k{}^2} \right), \qquad (\text{for } j \neq m)$$

$$h_{mj} = \sum_i \frac{a_{ij}{}^2}{n_i} \left(2 - \frac{\sigma_j{}^2}{n_i} \sum_j \frac{a_{ik}}{\sigma_k{}^2} \right) - \sum_i a_{ij}, \qquad (\text{for } j = m)$$

and

$$g_m = \sum_i \sum_j \frac{a_{ij} a_{im} \Delta M_{ij}}{n_i} \frac{\sigma_m^2}{\sigma_j{}^2} - \sum_i a_{im} \Delta M_{im}. \tag{14}$$

Now, there are N equations ($m = 1 \sim N$) for N unknowns (c_j, $j = 1 \sim N$). However, each equation in Eq.12 is not independent of the other. So, an extra equation must be introduced for c_j to make the equation set complete as,

$$\sum_j c_j = 0. \tag{15}$$

Combining Eq. 13 and Eq. 15, we can solve a set of linear equations and eventually get the values of the magnitude correction parameter for each station.

3 . 2 Results and Discussion on the Magnitude Correction

Using 2, 000 earthquakes which have occurred since September, 1988, and those stations which have contributed with reliable data, we could solve the linear equation set of Eq. 13 and Eq. 15 and obtain the station corrections for the magnitude determination. The parameter σ listed in Table 1 was applied for the parameter σ_j, σ_k and σ_m in Eq.14, which is a weighing factor for the data of each station in the calculation. The result is summarized in Table 2.

Figure 9 shows the geographical distribution of the classified station correction $-c_j$. It is revealed that in the western area bordered with the 139° E line, most of the stations have a positive correction value, which corresponds to the underestimation of the magnitude at those stations, and vice versa for the stations in the northern Kanto district, the Boso Peninsula, and the Izu Islands. Such correction factor can be caused first by surface effects around the local sites. Otherwise, there may be a possible effect attributable to the wide range tectonic structure, as proposed by Nakanishi and Horie (1980) .

Acknowledgements

I, M.T.Morandi, thank the NIED for providing this opportunity and facilities, and to all its staff for their hospitality. I also thank the IISEE staff for their hospitality and devotion during my stay in Japan, especially Dr. K. Ishibashi, the academic coordinator of the Seismology Course, 1989－1990. I would also like to thank JICA for its financial support. And finally, I would like to thank the authorities and the Faculty of the Department of Physics, University of Los Andes, Venezuela, for their support in my duties during my stay in Japan.

Table 2 Characteristic constants for magnitude. Oppositely signed value($-c$) corresponds to each station correction.

STATION	C	STATION	C
ABN	-0.14	ACH	-0.06
AKW	-0.18	ASG	0.09
ASY	0.16	CDP	-0.03
CHS	-0.03	CKR	-0.06
ENZ	-0.02	FCH	-0.54
FJM	0.02	FJW	-0.22
GER	-0.07	HAS	0.00
HCJ	0.39	HDA	-0.27
HHR	0.11	HKW	-0.18
HMO	0.00	HTN	0.36
HTS	0.03	ICH	0.29
IWT	-0.08	JIZ	0.06
KGN	-0.26	KGW	-0.29
KHZ	0.51	KIB	-0.01
KSH	-0.25	KTU	0.19
MIN	-0.21	MKB	-0.27
MKE	0.45	MNB	-0.15
MOR	0.69	MOT	0.54
MSK	-0.12	NJM	0.37
NMT	0.44	NMZ	-0.07
NRY	-0.16	ODK	-0.35
OHR	0.32	OHS	-0.14
OMM	0.34	OOH	0.30
OSM	0.00	SDM	-0.07
SHM	0.00	SIZ	-0.31
SMB	-0.24	SMD	-0.16
SMY	-0.12	SSN	0.61
SSW	-0.38	TNR	-0.15
TOE	0.09	TRU	-0.49
TR2	-0.28	TYM	0.37
USD	0.28	YKI	0.29
YMI	-0.36	YMK	-0.40
YSK	-0.22	YST	-0.01

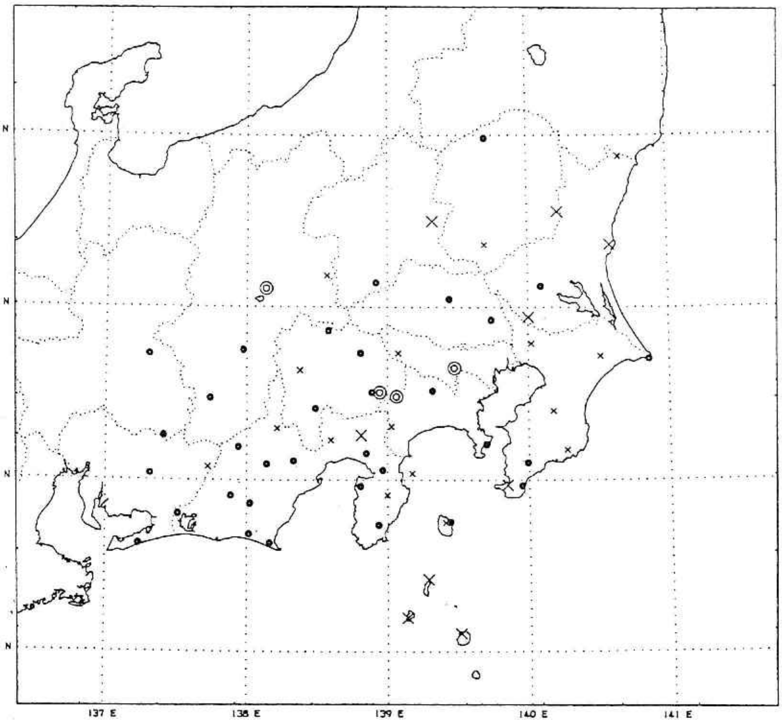

Fig.9 Distribution of station correction $-c_j$ for magnitude.
big double circle : $0.35 \leq -c_j < 0.70$,
small double circle : $0.00 \leq -c_j < 0.35$,
small cross : $-0.35 \leq -c_j < 0.00$,
big cross : $-0.70 \leq -c_j < -0.35$.

References

1) Hamada, K., Ohtake, M., Okada, Y., Matsumura,S. and Sato, H. (1985) :A high quality digital network for microearthquakes and ground tilt observations in the Kanto – Tokai area, Japan, Earthq. Predict.Res., **3** , 447–449.
2) Lee, W.H.K. and Stewart, S.W. (1981) :Principles and applications of microearthquake networks, edited by B.Saltzman, pp.1–293, Academic Press,Washington D.C.
3) Maeda, N. (1984) :On accuracy of magnitude determination –in case of maximum velocity amplitude magnitude–, ZISIN(Jour. Seism. Soc. Japan) **2** , **37** , 310 – 313(in Japanese with English Abstract).
4) Matsumura, S. (1984) :Evaluation of detection capability of microearthquakes for an observational network, ZISIN(Jour. Seism. Soc. Japan)**2** , **37** , 475–489(in Japanese with English Abstract).
5) Matsumura, S., Okada, Y., Shimada, S., Hori,S., Ohkubo,T., Imoto,M., Ohtake,M. and Hamada, K. (1986) :The analyzing system for precursors of earthquakes (APE) of the NRCDP, Japan, Proceedings of the 5th Joint Meeting of the UJNR Panel on Earthquake Prediction Technology, Tsukuba, Japan.
6) Nakanishi,I. and Horie,A. (1980) :Anomalous distributions of seismic intensities due to the descending Philippine Sea plate beneath the southern Kanto district, Japan, Journ. Phys. Earth, **28** , 333–360.

7) Papanastassiou,D. and Matsumura, S. (1987) :Examination of the NRCDP's seismic observational network as regards:I.Detectability－Locatability, II.Accuracy of the determination of earthquake source parameters, Report of Natl. Res. Cent Disast. Prev.,**39** , 37－65.

8) Ringdal,F. (1975) :On the estimation of seismic detection threshold, Bull. Seism. Soc. Am., **65** , 1631－1642.

9) Watanabe, M. (1971) :Determintion of earthquake magnitude at regional distance in and near Japan, ZISIN(Jour. Seism.Soc.Japan), **2** , **24** , 189－200(in Japanese with English Abstract).

(Manuscript Received December 20, 1990)

防災科学技術研究所における地震観測能力に関する最新の調査
―検知能力およびマグニチュード補正―

マリア・テレサ・モランディ* 松村正三**

要　旨

微小地震観測において一様観測の可能な領域がどの範囲まで広がっているかを調べることは極めて重要である．防災科学技術研究所の観測網については過去に既に二度にわたって地震の検知能力が調べられている．しかし，その後の観測網の充実や処理システムの改善によって検知能力は大きく変化したはずである．この報告では最新のデータに基づいて現時点での検知能力の再評価を行なった．その結果，従前に比較して関東地域の北部が広く高検知領域としてカバーされるようになっていることが判明した．しかし，房総半島を含む東南部の地域は依然として高感度の検知範囲から取り残されている．

また，ルーチン処理によって決められた平均マグニチュードから，個々の観測点の特性によってもたらされる効果を推定する手法を提案し，マグニチュードを算出する際の観測点補正値の決定を行なった．

*ロスアンデス大学（ベネズエラ）

JICA地震学コース研修員として1990年4月～7月防災科学技術研究所に滞在

**防災科学技術研究所地圏地球科学技術研究部